Viscoplastic Behavior and Modelization of an Austenitic Stainless Steel (17-12 SPH) at High Temperature (T = 600°C), Under In and Out of Phase Cyclic Tension-Torsion Loading

P. Delobelle

R. Lachat

Laboratoire de Mécanique Appliquée,
Faculté des Sciences et des Techniques,
Besancon Cedex, France

The results of experiments performed on an austenitic stainless steel of the type 316L at a temperature of 600°C are presented. The tests were made under both unidirectional (1D) and bidimensional (2D) cyclic tension-torsion loading, both in and out of phase with one (case of 2D ratchet) or two cyclic components. For the 2D loadings, it is shown that a weak supplementary hardening ΔH^+ appears which is mostly a function of the degree of phase difference φ between the strain components and the ratio R between the maximum amplitudes of these components. These observations conform qualitatively to those already reported for ambient temperature but quantitatively it is shown that the maximum amplitude of this supplementary hardening is a strongly decreasing function of the temperature. A simple phenomenological formulation is proposed which, when integrated into a unified viscoplastic model developed elsewhere, leads to a correct representation of the experimental results.

I Introduction

Since the advent of hydraulic tension-torsion machines ten years ago, experimental studies of the behavior of metallic materials under cyclic biaxial loadings [1-19] have developed significantly. Paradoxically, nearly all this work has been performed at ambient temperature [1-9], [12-15], [19]. This fact is certainly due to the difficulty of designing and fabrication a high temperature extensometer.

In the case of austenitic stainless steels [4-7], [10-19], it has been shown that a very significant supplementary hardening appears under cyclic biaxial loadings that is directly due to the phase difference between the components of the strain and to the ratio between the maximum amplitudes of these components. However, these steels are principally used under high temperature conditions and it seems interesting to study what happens at elevated temperatures to the different properties related to the biaxial state and observed at ambient temperature. It is thus proposed to study and model the cyclic behavior of this steel at 600°C for uniaxial and biaxial loadings. Since the effects of viscosity are present at this temperature, the influence of the loading rate on the stabilized state will also be studied.

Contributed by the Materials Division for publication in the JOURNAL OF ENGINEERING MATERIALS AND TECHNOLOGY. Manuscript received by the Materials Division November 29, 1990; revised manuscript received July 20, 1992. Associate Technical Editor: K. V. Jata.

II Experimental Methods

1) The Test Samples. The test pieces are obtained from slices taken from a 30 mm thick sheet, hyper-quenched from 1200°C. The microstructure is entirely austenitic and the average diameter of the grains is 45 μm. The weight composition of this steel is given in Table 1.

The tension-torsion specimens have a tubular geometry. Their outside and inside radii are, respectively, 5 and 4 mm and they have a gage length of 40 mm.

2) The Test Machines. The various biaxial tests have been conducted on a Schenck hydraulic tension-torsion machine whose maximum force and torque capacities are respectively 63 KN and 1000 Nm. The two analogical control signals are delivered by a H.P. function generator which itself can be controlled by a micro-computer. In this way, any periodic signal can be generated. The command of the strain is effected from signals delivered by a high temperature extensometer directly attached to the specimen [20].

The tension-torsion ratchet tests and certain cyclical torsion

Table 1 Weight composition of the 17-12 Mo SPH steel

C	S	P	Si	Mn	Ni	Cr	Mo	N	B	Co	Cu
≤0.03	≤0.001	≤0.021	0.44	1.08	12.3	17.54	2.47	0.075	0.001	0.15	0.175

Ti	Nb	Al	Ta	Fe
<0.005	0.015	0.100	—	Bal.

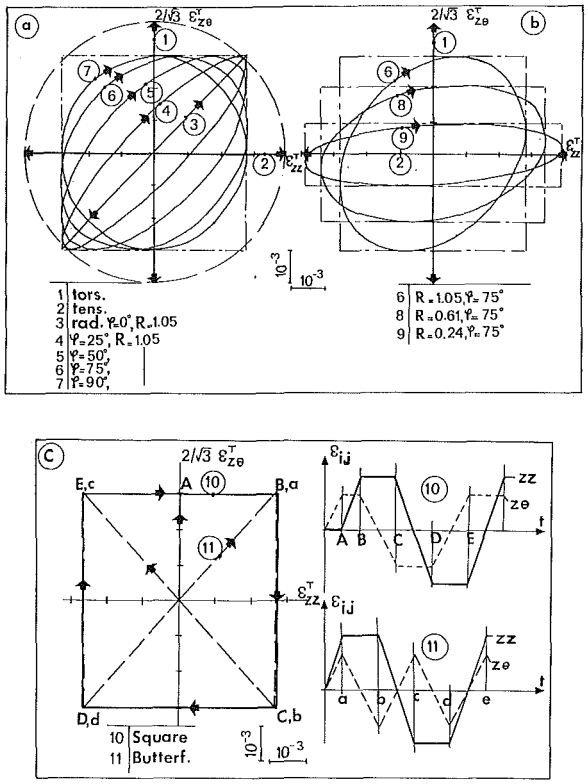

Fig. 1 Various cyclic loading paths in the equivalent Von-Mises strain space ($(2/\sqrt{3})\epsilon^T_{z\theta}$, ϵ^T_{zz})

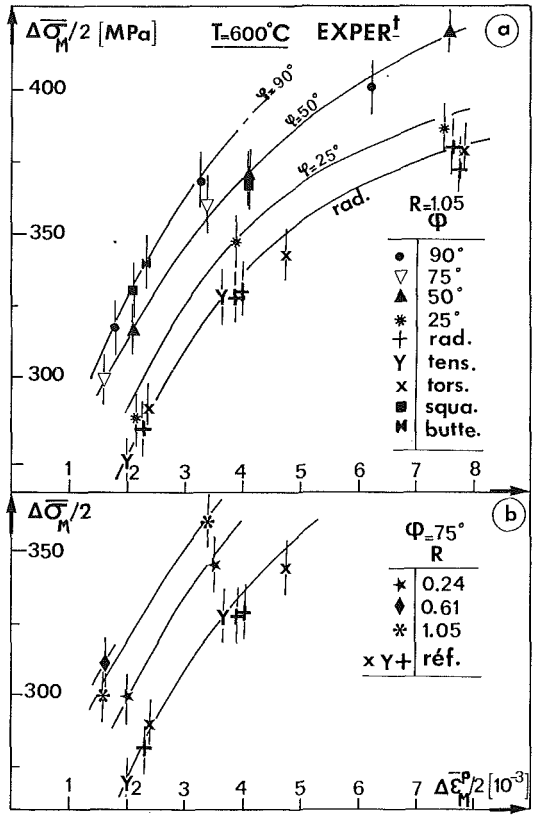

Fig. 2(*a*) Influence of the phase difference on the cyclic hardening curve at T = 600°C. (*b*) Influence of the ratio $R = (2\epsilon^T_{z\theta}m)/(\sqrt{3}\epsilon^T_{zz}m)$, on the cyclic hardening curve.

tests have been performed on a controlled electrodynamic machine.

3) The Experimental Procedure. All the tests have been performed at imposed total strains. For the uniaxial tests, a triangular signal is generated and the period is varied in a discrete manner in the ratio 10^3. For a part of the biaxial tests, the strain signals for the tension and torsion components are sinusoidal and such that:

$$\epsilon^T_{zz} = \epsilon^T_{zz}m\sin\omega t$$
$$\epsilon^T_{z\theta} = \epsilon^T_{z\theta}m\sin(\beta t - \varphi) \qquad (1)$$

ω is the angular frequency equal to $1.88\ 10^{-2}$, which corresponds to an equivalent strain rate, in the sense of Von-Mises, on the order of $4.8\ 10^{-5}\ s^{-1}$. φ is the phase difference between the two components and $\epsilon^T_{zz}m$, $\epsilon^T_{z\theta}m$ are the maximum amplitudes. In order to study the respective influences of φ and of the ratio $R = (2\epsilon^T_{z\theta}m/\sqrt{3}\ \epsilon^T_{zz}m)$, two series of tests have been performed with: $R \simeq 1$ and φ = 0, 25, 50, 75, 90 deg, (Fig. 1(*a*)) and with: $\varphi = 75°$ and $R \simeq 0$, 0.25, 0.61, 1 (Fig. 1(*b*)). In addition, while conserving these characteristics, each specimen has been tested with two levels of maximum strain am-

Nomenclature

$\dot{X}$ = derivative of the variable X with respect to time
δ_{ij} = Kronecker delta
$H(X)$ = Heaviside function, $H(X) = 1$ if $X \geq 0$ and $H(X) = 0$ if $X < 0$
$\langle X \rangle$ = Macauley brackets, $\langle X \rangle = XH(X)$

Multiaxial strains:

ϵ^T_{ij}, ϵ^T_{ij}, ϵ^v_{ij} = total, elastic, viscoplastic components of the strains tensors
$\dot{\bar{\epsilon}}^v$ = $\dot{\bar{\epsilon}}^v = \{2/3(\dot{\epsilon}^v_{ij}\dot{\epsilon}^v_{ij})\}^{1/2}$, Von Mises equivalent strain rate
q^* = $q^* = \int_0^t \sqrt{2/3}\ (\dot{\epsilon}^v_{ij}\dot{\epsilon}^v_{ij})^{1/2}dt$, cumulated viscoplastic deformation
$\overline{\epsilon^v - \xi}$ = $\epsilon^v - \xi = (2/3(\epsilon^v_{ij} - \xi_{ij})\,(\epsilon^v_{ij} - \xi_{ij}))^{1/2}$, second invariant of the $\epsilon - \xi$ tensor
$\bar{\epsilon}^v$ = $\bar{\epsilon}^v = (2/3(\epsilon^v_{ij}\ \epsilon^v_{ij}))^{1/2}$, Von Mises equivalent strain
n^*_{ij} = $n^*_{ij} = \sqrt{2/3}((\epsilon^v_{ij} - \xi_{ij})/\overline{\epsilon^v - \xi})$, exterior normal to G

Multiaxial stresses:

σ_{ij} = applied stress components
σ'_{ij} = $\sigma'_{ij} = \sigma_{ij} - (\delta_{ij}/3)\sigma_{kk}$, deviatoric stress components
$\bar{\sigma}$ = $\bar{\sigma} = (3/2(\sigma'_{ij}\sigma'_{ij}))^{1/2}$, Von Mises equivalent stress
$\overline{\sigma - \alpha}$ = $\overline{\sigma - \alpha} = \{3/2(\sigma'_{ij} - \alpha'_{ij})(\sigma'_{ij} - \alpha'_{ij})\}^{1/2}$, Von Mises equivalent effective stress
$\alpha^{(i)}_{ij}$ = internal kinematical variables components (ith variable)
$\bar{\alpha}$ = $\bar{\alpha} = (3/2(\alpha'_{ij}\alpha'_{ij}))^{1/2}$, Von Mises equivalent kinematic variable
n_{ij} = $n_{ij} = (\sqrt{3/2}\ (\sigma'_{ij} - \alpha'_{ij})/\overline{\sigma - \alpha})$, normal exterior to the equipotentiel surfaces

Other used symbols are defined in the text, when introduced.

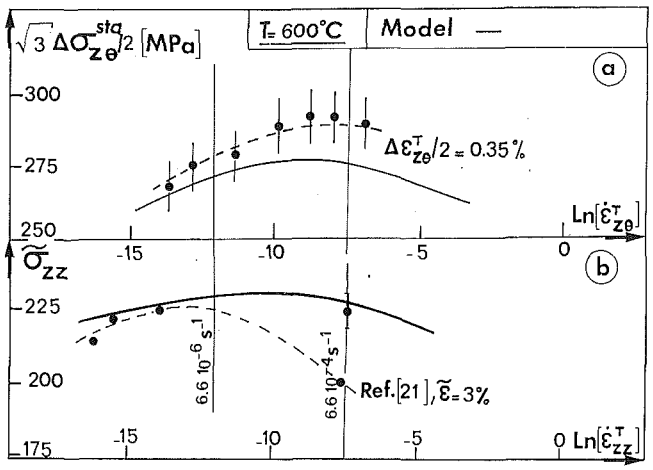

Fig. 3 Influence of loading rate on the stress at the stabilized cyclic. (*a*) Experiments and simulations. (*b*) Idem for the monotonic tension curve.

plitudes, successively increasing and such that a ratio of approximately 1.5 is maintained between the components of the two levels. One hundred cycles are performed at each level in such a way as to clearly define the stabilized state.

The influence of an arbitrary cyclic loading, where the notion of phase difference is not clearly defined, has also been tested by using imposed cycles in the form of squares or butterflies with, as previously, $R \simeq 1$. The waveform of the imposed signals is generated from ramps defining triangles and trapezoids (Fig. 1(*c*)).

For the 2D ratchet tests, the experimental sequence consists in applying a weak axial tensile stress σ_{zz} and in the superposition of a cyclic torsional strain of constant amplitude $\Delta\epsilon^T_{z\theta}$ and for a fixed strain rate $\dot{\epsilon}^T_{z\theta}$. This type of nonradial loading has the advantage of making a progressive strain appear along the axial direction, which can lead, as will be seen later, to some conclusions concerning the formulation of nonradial effects. The test parameters are such that: $\sigma_{zz} = 50$ MPa, $\Delta\epsilon^T_{z\theta}/2 = \pm 0.35$ percent and $\dot{\epsilon}^T_{z\theta} = 4.6\ 10^{-5}\ s^{-1}$.

III Experimental Results

1) Uniaxial Tests. It is well-known that austenitic stainless steels present, even at high temperatures, a strong cyclic hardening. The experimental data points reported in Fig. 2(*a*) result from tension or torsion tests with an equivalent strain rate of the order of $4.6\ 10^{-5}\ s^{-1}$ and define the cyclic hardening curve: $\Delta\bar{\sigma}_M/2 = f(\Delta\bar{\epsilon}^p_M/2)$. For the stabilized cycle, the coordinates of the points $\Delta\sigma_M/2$ and $\Delta\bar{\epsilon}^p_M/2$ are the maximum equivalent stress and plastic strain in the sense of Von-Mises, respectively, i.e., for torsion: $\Delta\sigma_M/2 = \sqrt{3}\ \Delta\sigma_{z\theta}/2$ and $\Delta\bar{\epsilon}^p_M = (2/\sqrt{3})\ \Delta\epsilon^p_{z\theta}/2$.

In Fig. 3(*a*), the influence of the loading rate $\dot{\epsilon}^T_{z\theta}$ on the equivalent stress at the stabilized cycle ($\sqrt{3}\ \Delta\sigma^{sta}_{z\theta}/2$) is represented in the case of a torsion test ($1.4\ 10^{-6} \leq \dot{\epsilon}^T_{z\theta} \leq 1.4\ 10^{-3}\ s^{-1}$). The effects of viscosity are thus made apparent, the sensitivity coefficient of the stress to the strain rate, $n^* = ((\partial\Delta\bar{\sigma}/2)/\partial \mathrm{Ln}\ \dot{\epsilon}^T_{z\theta})$, being positive. However, for higher loading rates, the slope has the tendency to change sign, this effect being confirmed by the results of monotonic tests obtained on a very similar steel [21] and reported in Fig. 3(*b*). At lower temperatures ($200 \leq T \leq 500$°C) and for the same series of loading rates, the coefficient n^* is in fact negative [22-24]. This behavior is directly related to the Portevin-Le Chatelier effect and is attributed to the short distance interactions between the dislocations and the point defect configurations [23-24]. For this study, it is necessary to take into account the rate

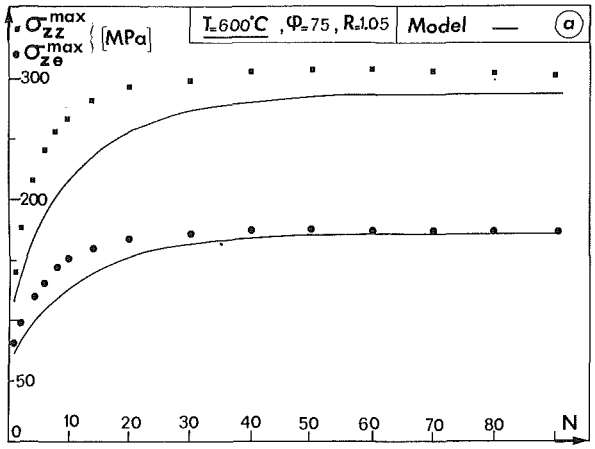

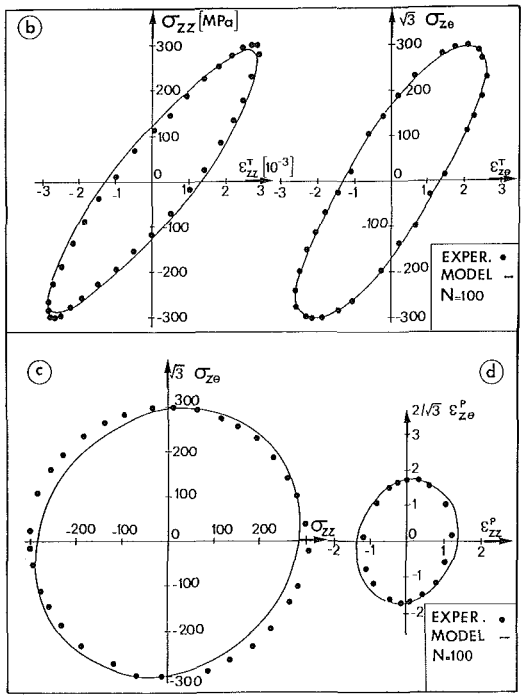

Fig. 4 Test under sinusoidal sollicitations, such that $\varphi = 75$ deg and $R = 1.05$. (*a*) Evolution of the maximum stresses ($\sigma^{max}_{z\theta}$, σ^{max}_{zz}) as a function of the number of cycles *N*. Experiments and simulations; (*b*) Evolution of the cycles, $\sqrt{3}\sigma_{z\theta} = f(\epsilon^T_{z\theta})$ and $\sigma_{zz} = f(\epsilon^T_{zz})$ for the same loading. Experiment and simulations; (*c*) Stress paths in the plane ($\sqrt{3}\sigma_{z\theta}$, σ_{zz}). Experiment and simulation; (*d*) Plastic strain paths in the plane ($2/\sqrt{3}\epsilon^p_{z\theta}$, ϵ^p_{zz}). Experiment and simulation

effects for a precise description of the sinusoidal tests in which the strain rates vary in a significant manner. Note that, for other isotherms, this rate dependence is generally different [24]. Though the omission of these rate effects would lead to errors of only a few percent (< 5 percent) in this particular study, this would not be the case for anisothermal loadings where the rate factor is an important parameter, particularly in the neighborhood of 550°C [24]. Since the modelization presented here is meant to be fairly general and the case of anisothermal loading is currently under development, the previously described effects should not be neglected.

2) The Biaxial Tests

i) Case of Imposed Cyclic Strains. The simultaneous evolutions of the various test characteristics are enregistered during the hardening in both an analogical and numerical fashion. Three examples corresponding to an elliptical, a butterfly and

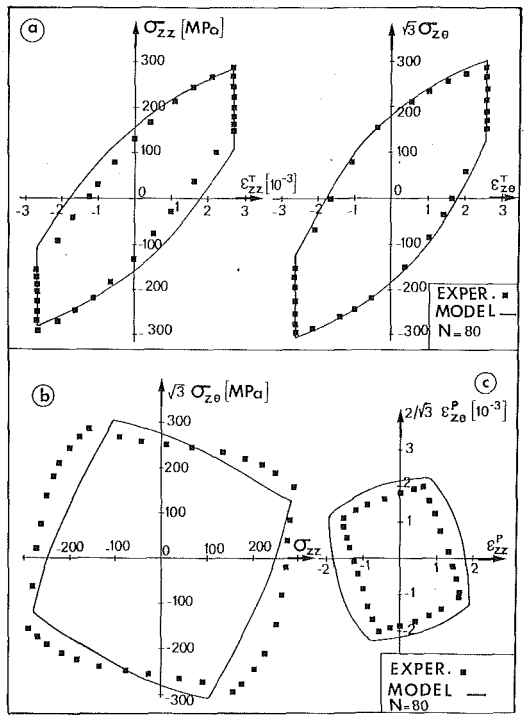

Fig. 5 Loading path in the form of a butterfly with $R \simeq 1.15$. (*a*) Evolution of the cycles ($\sqrt{3}\sigma_{z\theta} = f(\epsilon^T_{z\theta})$ and $\sigma_{zz} = f(\epsilon^T_{zz})$). Experiments and modelizations. (*b*) Stress paths in the plane ($\sqrt{3}\sigma_{z\theta}$, σ_{zz}). Experiment and simulation. (*c*) Plastic strain paths in the plane ($2/\sqrt{3}\epsilon^p_{z\theta}$, ϵ^p_{zz}). Experiment and simulation.

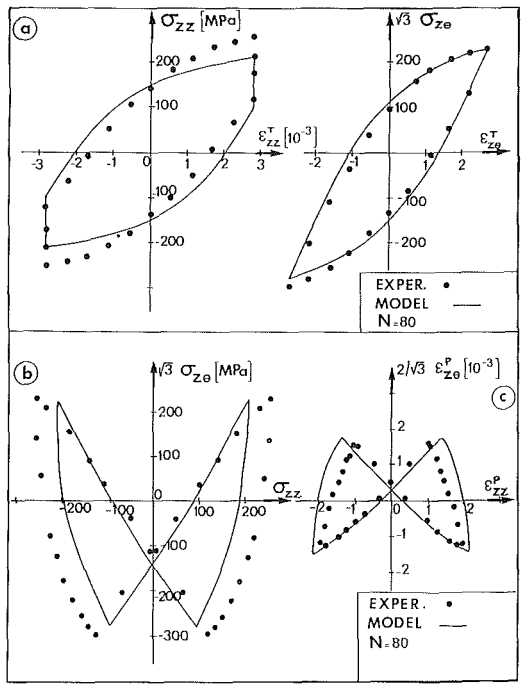

Fig. 6 Loading path in the form of a square with $R \simeq 1$. (*a*) Evolution of the cycles ($\sqrt{3}\sigma_{z\theta} = f(\epsilon^T_{z\theta})$ and $\sigma_{zz} = f(\epsilon^T_{zz})$). Experiments and modelization. (*b*) Stress paths in the plane ($\sqrt{3}\sigma_{z\theta}$, σ_{zz}). Experiment and modelization. (*c*) Plastic strain paths in the plane ($2/\sqrt{3}\epsilon^p_{z\theta}$, ϵ^p_{zz}). Experiment and modelization.

a square paths are respectively presented on Fig. 4 to 6. The following parameters can thus be determined:

—The maximum attained stress in each direction (σ^{max}_{zz} and $\sigma^{max}_{z\theta}$) as a function of the number of cycles N (Fig. 4(*a*)).

—The evolution of the tension and torsion cycles, which allows the form of the loops for the stabilized cycles to be obtained (Fig. 4(*b*), 5(*a*) and 6(*a*)).

—The path, for the stabilized cycles, of the components of the stress in the equivalent Mises plane (Fig. 4(*c*), 5(*b*), and 6(*b*)).

—The path, for the stabilized cycles, of the components of the plastic strain in the equivalent Mises plane (Fig. 4(*d*), 5(*c*), and 6(*c*)). The plastic strains $\epsilon^p_{ij}(t)$ are determined from the simultaneous knowledge of the imposed total deformations $\epsilon^T_{ij}(t)$ and the stresses $\sigma_{ij}(t)$, hence:

$$\left.\begin{aligned}\epsilon^P_{zz}(t) &= \epsilon^T_{zz}(t) - \sigma_{zz}(t)/E\\ \epsilon^P_{z\theta}(t) &= \epsilon^T_{z\theta}(t) - \sigma_{z\theta}(t)/2G\end{aligned}\right\} \quad (2)$$

E and G are, respectively, Young's modulus and the shear modulus. Thus, for the stabilized cycles and in the two equivalent Mises planes, the maximum stress $\overline{\Delta\sigma}_M/2$ and strain $\overline{\Delta\epsilon}^P_M/2$ correspond geometrically to the radii of the two smallest circles containing the paths. The couples $\overline{\Delta\sigma}_M/2 = f(\Delta\epsilon^P_M/2)$ for all the tests described precedently are reported in Fig. 2.

In this way it is shown that a supplementary hardening due to the phase difference between the strain components appears, as it did for ambient temperature. This supplementary hardening is quantified by the parameter ΔH^+, which is equal to the difference between $(\overline{\Delta\sigma}_M(\varphi, R)/2)$, for φ and R fixed, and $\overline{\Delta\sigma}_M/2$ for a uniaxial test (tension or torsion) for the same equivalent plastic strain. Figure 7 shows the influence of φ and R on ΔH^+ for two levels of plastic strain ($\overline{\Delta\epsilon}^P_M/2 = 2\ 10^{-3}$ and $3.7\ 10^{-3}$). The points obtained by Murakami et al. [17] at 600°C on a similar steel are also reported.

Like at ambiant temperature, ΔH^+ is nearly zero for $\varphi =$

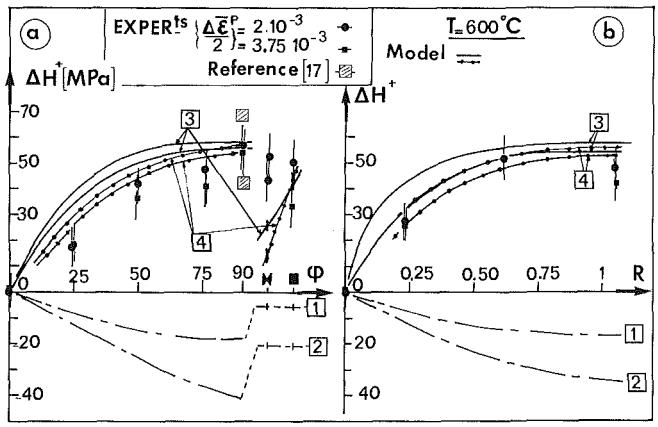

Fig. 7(*a*) Evolution of the parameter ΔH^+ with the phase difference φ. (*b*) Evolution of the parameter ΔH^+ with the ratio R. Experiments and simulations.

0 and maximum for $\varphi = 90$ deg. In the same way, for φ fixed, ΔH is maximum for $R \simeq 1$ ($R = 2/\sqrt{3}$) [5-6] [12-15]. It is also shown that the shape of the curve conforms to those reported at 20°C [12] [15] and that the maximum hardening is nearly obtained from $\varphi \simeq 50°$ and upwards. It can be also shown that this hardening is totally evanescent when the phase difference is eliminated. For the square path, ΔH^+ is on the order of the maximum hardening, which also corroborates the remarks made for ambient temperature [5-6], [13], [15]. In conclusion, it has just been shown that, qualitatively, the responses of this steel to biaxial loading are identical at 20°C and 600°C. However, while the maximum supplementary hardening is on the order of 230 MPa at 20°C for $\overline{\Delta\epsilon}^P_M/2 \simeq 4\ 10^{-3}$ [12], [15], it only reaches 60 MPa at 600°C for the same strain amplitude.

From a physical point of view, this supplementary hard-

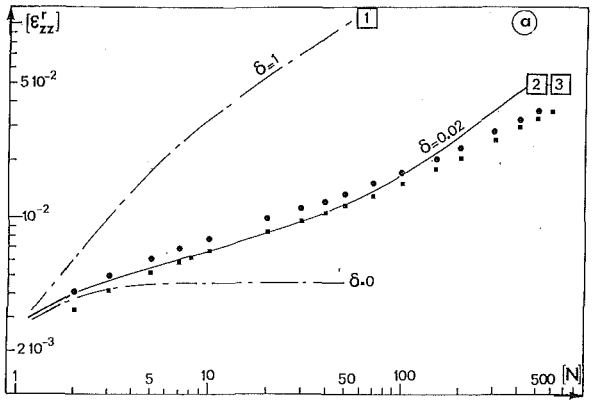

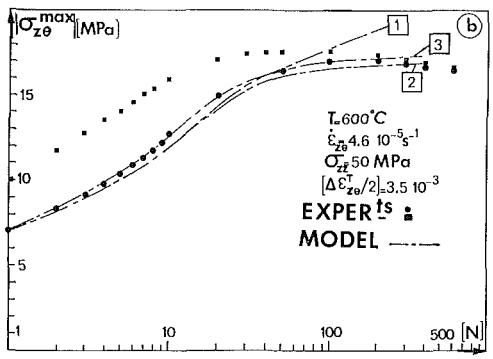

Fig. 8(*a*) Evolution of the progressive strain ϵ^r_{zz} with the number of cycles *N*. Experiments and modelization. (*b*) Evolution of the maximum stress $\sigma^{max}_{z\theta}$ with the number of cycles *N*. Experiments and modelizations.

ening, caused by the rotation of the stresses, is certainly due on the one hand, to the activation of new secondary gliding systems favorably oriented with respect to the stress components and, on the other hand, to the interactions between the different activated systems [19], [25]. However, for these steels the stacking fault energy is an increasing function of the temperature and thus the escape by cross-slip becomes possible. In addition, taking into account the elevated levels of the developed internal stresses, the climbing escape is also possible. These two mechanisms, can explain the strong decrease of ΔH^+ with the temperature.

(*ii*) *Case of Tension-Torsion Ratchet.* The response of a material submitted to this type of loading consists in the appearance of a progressive axial strain ϵ^r_{zz} (Fig. 8(*a*)) due to the axial and shear stresses and in a cyclic hardening in the direction of the shear component (Fig. 8(*b*)). It can be remarked that the ratchet strain is permanent and that the stress for the stabilized cycle corresponds in the limits of experimental accuracy to the stress obtained in pure torsion. This last point shows the insensitivity of the non-radiality effect to the progressive strain since this weakly non-radial loading remains during the span of the test. The theoretical definition of the notion of nonradiality should take into account this property.

IV Phenomenological Modelization

In this section, a phenomenological formulation is proposed of the two principal effects described in Section III. These equations are then integrated into a unified viscoplastic model developed elsewhere and already identified at the isotherm 600°C for diverse monotonic and cyclic unidirectional loadings [23-24], [18]. The meaning of the different terms or parameters of the equations is given in the nomenclature.

IV.1. Review of the Initial Formulation of the Model

(*i*) *The Strain Rates.* The total strain ϵ^T_{ij} can be decomposed into two components, respectively, elastic ϵ^e_{ij} and viscoplastic ϵ^v_{ij}. The rates of these components are such that:

$$\dot{\epsilon}^T_{ij} = \dot{\epsilon}^e_{ij} + \dot{\epsilon}^v_{ij} \tag{3}$$

$$\dot{\epsilon}^e_{ij} = \frac{1+\nu}{E}\,\dot{\sigma}_{ij} - \frac{\nu}{E}\,\delta_{ij}\dot{\sigma}_{kk}, \tag{4}$$

$$\dot{\epsilon}^v_{ij} = \frac{3}{2} f(\overline{\sigma-\alpha})\,\frac{\sigma'_{ij}-\alpha'_{ij}}{\overline{\sigma-\alpha}}\,\dot{} \quad \text{and} \quad f(\overline{\sigma-\alpha})$$

$$= \dot{\epsilon}_0 \left(\frac{N(\bar{\epsilon})}{\sigma^*_0}\right)^n \sinh\left(\frac{\overline{\sigma-\alpha}}{N(\bar{\epsilon})}\right)^n \tag{5}$$

$$N(\bar{\epsilon}) = CY + C^+ Y^+ \tag{6}$$

$\dot{\epsilon}_0$, σ^*_0, n, C and C^+ are five material constants fixed for a given isotherm and $N(\bar{\epsilon})$ is a function of the scalar variables Y and Y^+ described in the following.

(*ii*) *The Variables of Kinematic Hardening.* The kinematic tensor variable α_{ij} represents the sum of the internal stresses induced by the interactions at different distances between the mobile dislocations and those of the substructure. To describe these different interaction scales, several nonlinear kinematic variables having different kinetics are used [24], [27-29], hence:

$$\left.\begin{aligned}
\dot{\alpha}_{ij} &= p_m\left(\frac{2}{3}(Y^*+Y^+)\,\dot{\epsilon}^v_{ij} - (\alpha_{ij}-\alpha^{(1)}_{ij})\,\overline{\dot{\epsilon}}^v\right) \\
&\qquad - R_m(\sinh\beta(\overline{\alpha})^{M1})^{M0}\,\frac{\alpha_{ij}}{\overline{\alpha}} \qquad (a)\\
\dot{\alpha}^{(1)}_{ij} &= p_1\left(\frac{2}{3}\,Y^*\,\dot{\epsilon}^v_{ij} - (\alpha^{(1)}_{ij}-\alpha^{(2)}_{ij})\,\overline{\dot{\epsilon}}^v\right) \qquad (b)\\
\dot{\alpha}^{(2)}_{ij} &= p_2\left(\frac{2}{3}\,Y^*\,\dot{\epsilon}^v_{ij} - \alpha^{(2)}_{ij}\,\overline{\dot{\epsilon}}^v\right) \qquad (c)
\end{aligned}\right\} (7)$$

with the initial values, $\alpha(0) = \alpha^{(1)}(0) = \alpha^{(2)}(0) = 0$. p_m, p_1, p_2, β, R_m, M_0 and M_1 are material constants. It is remarked that the scalar variable Y^* and Y^+ describe the evolution of the asymptotic state of each of these variables.

(*iii*) *The Scalar Hardening Variables Y^* and Y^+.* Taking into account the ulterior developments, let Y^* initially be defined by $Y^* = Y$. The scalar variables are generally introduced in the models to describe the cyclic properties of the materials and are directly related to the increase of the total density of dislocations. These variables depend essentially on the accumulated plastic strain and can be written:

$$\left.\begin{aligned}
\dot{Y} &= b(Y^{sat}-Y)(\overline{\dot{\epsilon}}^v - R|Y-Y_0|^{L0}\,\mathrm{sign}(Y-Y_0)) \\
&\qquad \text{with } Y(0)\neq 0 \qquad (a)\\
\dot{Y}^+ &= b^+(Y^{sat+}-Y^+)(H(G^+)\,\overline{\dot{\epsilon}}^v \\
&\qquad - R^+|Y^+-Y^+_0|^{L0}\mathrm{sign}(Y^+-Y^+_0)) \\
&\qquad \text{with } Y^+(0)\neq 0 \qquad (b)
\end{aligned}\right\} (8)$$

b, b^+, R, R^+, R_0, and L_0 are material constants and Y_0, Y^+_0 (Eq. (9)) represent the nonrecoverable parts of Y and Y^+.

$$\left.\begin{aligned}
Y_0 &= \mathrm{Max}(Y-(1/3)(R_0/R)^{1/L0}(\sinh\beta(\mathrm{Max}\overline{\alpha})^{M1})^{M0/L0}) \qquad (a)\\
Y^+_0 &= \mathrm{Max}(Y^+-(R_0/R^+)^{1/L0}(\sinh\beta(\mathrm{Max}\overline{\alpha})^{M1})^{M0/L0}) \qquad (b)
\end{aligned}\right\} (9)$$

Y^{sat} given by Eq. (12) is a partial memorization function of the largest plastic strain and $H(G^+)$ is defined by Eq. (10).

(*iv*) *Memorization Function of the Plastic Deformation.* For these steels, the amplitude of the cyclic hardening depends essentially on the amplitude of the imposed strain, in other words, that the asymptotic value Y^{sat} of variable Y depends on the amplitude of the strain [18], [30]. This effect is modelized by postulating the existence of non-hardening surfaces G and G^+ expressed in the strain space [28], [30–32]:

$$G = \overline{\epsilon^v - \xi} - q \leq 0, \text{ and } G^+ = \bar{\epsilon}^v - q^* \leq 0 \tag{10}$$

The evolution of the center ξ_{ij} and the radius q of the surface G are given by:

$$\left.\begin{aligned} \dot{q} &= \eta H(G) < n_{ij} n^*_{ij} > \dot{\bar{\epsilon}}^v \quad (a) \\ \dot{\xi}_{ij} &= \sqrt{3}/2((1-\eta)H(G) < n_{ij} n^*_{ij} > n^*_{ij} \dot{\bar{\epsilon}}^v) \quad (b) \end{aligned}\right\} \tag{11}$$

The variable q governs the growth of the saturation value Y^{sat}, so:

$$\dot{Y}^{sat} = b^{sat}(Y^{sat}_{\infty} - Y^{sat})\dot{q} \text{ with } Y^{sat}(0) \neq 0 \tag{12}$$

As was remarked earlier, the precise modelization of the rate effects ($n^* \gtrless 0$) requires that the interaction phenomena between dislocations and point defects be taken into account. Toward this end, a phenomenological approach is presented resulting from an experimental study of the yield point return after aging under stress [23], [24]. This step being accomplished, the predictions of the model can be compared to the out of phase test results and new improvements can eventually be proposed.

IV.2 Modelization of the Rate Effects. Even though there exist significant agreement in attributing the physical origin of a negative loading rate sensitivity to the dislocation-point-defect interactions, the phenomenological approach has paradoxically received very little attention [23], [37–39] and requires a brief elucidation. In the temperature domain 20–700°C, it has been possible to identify five elementary mechanisms of short distance interaction which contribute in an additive manner to the global material hardening [23], [36–40]. In the general context of internal variable models, a scalar component $Y^{(i)}$ can be attributed to each interaction (i), which is governed by the following equation:

$$\dot{Y}^{(i)} = -p^{(i)} Y_{(i)} \dot{\bar{\epsilon}}^v + \frac{Y^{(i)}_{\infty} - Y^{(i)}}{\tau^{(i)}_{SN}} \text{ with } i \in [1, 5] \tag{13}$$

In this equation, for a given interaction, $p^{(i)}$ is a constant, $\tau^{(i)}_{SN}$ the thermally activated relaxation time intrinsic to the interaction under consideration, and $Y_{(i)\infty}$ its efficiency function. This equation predicts, in agreement with experience a first order time hardening, exponentially evanescent with the strain. The stabilized regime of this equation ($\dot{Y}^{(i)} = 0$) is a decreasing function of the strain rate. These interactions are closely related to the spatial distribution of the cluster of point defects in the stress field of the dislocations and are thus a function of the density of the latter represented by the scalar variable Y. It remains then to relate this variable to the interaction spectrum which is a function of the total fraction of reoriented atoms y_c, hence:

$$Y^* = Y(1 + \gamma_c y_c) \text{ with } y_c = \sum_{(i)} Y^{(i)} \text{ and } i \in [1, 5] \tag{14}$$

where γ_c is a constant. In the kinematic variable Eqs. (7), the variable Y^* is given by Eqs. (14) and in general, $Y^* \neq Y$. For the isotherm 600°C, there is only one active interaction, that is to say, $i = 1$ in Eq. (14) [37]. In this case, this new formulation introduces only four supplementary parameters.

Figure 3 shows the predictions of the model vis-a-vis the rate effects for cyclic and monotonic loadings. The agreement is satisfactory and it is shown that a maximum can be obtained resulting from antagonistic effects of the normal viscosity ($n^* > 0$) and the interactions ($n^* < 0$). Note that the sensitivity coefficient n^* is correctly modeled as negative at lower temperatures ($200 \leq T < 550$°C) for the same range of loading rates, while for 20 and 650°C it is positive [24] [37].

IV.3 Modelization of the Out of Phase Tests. As might be expected, an examination of the model predictions with respect to the non-proportional effects (Fig. 7(*a*, *b*), curves 1) shows that the supplementary hardening ΔH^+ cannot be correctly handled. A light softening is even obtained ($\Delta H^- < 0$) due to the noncolinearity between the three kinematical components.

In the case of 2-D ratchet, the progressive axial strain is significantly overestimated while the cyclic hardening along the shear component is only slightly overestimated (Fig. 8, curves 1). In order to correct these defaults, it is necessary, to define a new parameter related to the state of non-proportionality.

(*i*) *Description of the 2-D Ratchet.* For this type of loading, it is clearly shown [18] that the progressive strain is due to a flow normal to the equipotential surfaces kinematically translated in the stress space. Thus, acting on the position of the kinematic variables by the intermediary of the evanescent terms, the flow direction and as consequence the amplitude of the progressive strain can be modified. Toward this end, Burlet and Cailletaud [41] have introduced the notion of radial evanescence and this leads to the shakedown at the end of a certain number of cycles. Following this idea, the kinematic variable $\alpha^{(2)}_{ij}$ (Eq. (7*c*)), which controls the evolution of α_{ij} can be redefined in the form [42]:

$$\dot{\alpha}^{(2)}_{ij} = p_2 \left(\frac{2}{3} Y^* \dot{\epsilon}^v_{ij} - (\delta \alpha^{(2)}_{ij} + (1-\delta)(\alpha^{(2)}_{ij} n_{ij}) n_{ij}) \dot{\bar{\epsilon}}^v \right) \tag{15}$$

For $\delta = 0$, there is a radial evanescence, while $\delta = 1$ results in the normal evanescence described by Eq. (7*c*). In the unidirectional case, for any value of δ, the well known nonlinear kinematic hardening relation is obtained. In the present state of the model with $\delta = 0.02$, it is shown (Fig. 8, curves 2) that the progressive strain and the evolution of the cyclic hardening are perfectly described.

(*ii*) *Description of the Imposed Strain Tests.* The new definition of $\alpha^{(2)}_{ij}$ also affects the model's response to cyclic out of phase loadings and accentuates the defaults mentioned earlier, notably that a parameter $\Delta H^- < 0$ (Fig. 7, curves) is obtained. However, it is remarked that the forms of the different stress and plastic strain loops are qualitatively described fairly well, and only the intervention of a homothetic factor, as a function of the phase difference, would be able to describe the experimental reality. This observation tends to show that the introduction of a new scalar quantity which is a function of the phase difference should be sufficient [15], [43]. A scalar variable Y_θ is thus introduced, representing the increase in density of the dislocations due to the activation of secondary systems, and allowing the redefinition of the variable Y^*, such that:

$$Y^* = (Y + Y_\theta)(1 + \gamma_c y_c) \tag{16}$$

Thus, the amplitude of the supplementary hardening is also a function of the loading rate. This hypothesis seems physically acceptable but remains to be verified by studying experimentally the influence of the strain rate on the parameter ΔH^+. It should be noted that the unanimity is realized in terms of the introduction of a scalar function in order to describe the effects of nonradiality [8–9], [11–12], [14–15]. The definition of a phase difference parameter θ, such that $0 \leq f(\theta) \leq 1$ for $0 \leq \varphi \leq 90$ deg is much too ambiguous and no agreement

has come out of the totality of the works. In fact, for a non-radial loading, a tensor quantity X_{ij} is out of phase, on the one hand, with its own derivative $\dot{X}_{ij}$ and, on the other hand, with the other tensor quantities Z_{ij} and their derivatives $\dot{Z}_{ij}$. It is thus possible to define a set of angles θ. Among these different possibilities, several tensor products have been proposed [11–12], [15], [44+46].

The choice of a particular angle can only be made from a correlation between the predictions obtained using different angles and the experimental results coming from the complex loading sequences. However, a decisive result presented by Benallal et al. [45], which agree with the results obtained in 2-D ratchet, is the indifference, as soon as a sufficient plastic strain is accumulated, of the stress paths in the equivalent Mises plane to the effects of the average strain, the other parameters being identical. It is recalled that this type of behavior has already been observed in this steel of uniaxial loadings; the relaxation of the average stress being total [47]. This observation allows the elimination of certain angles which are sensitive to the average strain.

In the present case, the procedure consists in systematically calculating, for the three type of non-radial loadings, (circular paths with and without average strain and 2D ratchet loading), all the possible angles and to compare them to the properties of these loadings in terms of the non-radiality. Following this correlation, only a few possible angles remain, notably:

$$\theta = \cos^{-1}\left(\frac{\sigma_{ij}}{\bar{\sigma}}\frac{\dot{\sigma}_{ij}}{\dot{\bar{\sigma}}} \text{ or } \frac{\alpha_{ij}}{\bar{\alpha}}\frac{\dot{\alpha}_{ij}}{\dot{\bar{\alpha}}}\right),$$

in addition to those defined by the cross-combinations ($\sigma_{ij}\dot{\alpha}_{ij}$, $\alpha_{ij}\dot{\sigma}_{ij}$). These two last possibilities can be eliminated as they are very close and symmetric with respect to the earlier solutions. Note that, only the 2D ratchet eliminate the ($n_{ij}n^*_{ij}$) possibility.

Only two angles remain which are defined by the applied stresses σ_{ij}, the internal stresses α_{ij}, and their derivatives $\dot{\sigma}_{ij}$, $\dot{\alpha}_{ij}$. This conclusion is in agreement with those of Bodner [44] and Benallal et al. [45]. The angles θ having been chosen, the kinetics of the variable Y_θ (Eq. (16)), which integrates the variations of this angle for a given cycle, can be written:

$$\dot{Y}_\theta = b_\theta(Y_\theta^{\text{sat}} f(\theta) - Y_\theta)\dot{\bar{\epsilon}}^v, \text{ with } Y_\theta(0) = 0 \text{ and}$$

$$\theta = \cos^{-1}\left(\frac{\sigma_{ij}}{\dot{\sigma}}\frac{\dot{\sigma}_{ij}}{\dot{\bar{\sigma}}} \text{ or } \frac{\alpha_{ij}}{\bar{\alpha}}\frac{\dot{\alpha}_{ij}}{\dot{\bar{\alpha}}}\right) \qquad (17)$$

For the choice of $f(\theta)$ two approaches are then possible: either the hardening deficit (ΔH^-) and excess (ΔH^+) are treated globally by the function $f(\theta)$ (model 1), or these two effects are treated separately, that is to say, first correct the effects due to the noncolinearity of the kinematical variables which is a function of the parameter δ, then use $f(\theta)$ to describe the hardening effects (model 2). These two approaches will be successively presented:

Model 1: While respecting the conditions evoked earlier, the function $f(\theta)$ can be empirically chosen in the form:

$$f(\theta) = 1 - |\cos\theta|^{n\theta} \qquad (18)$$

This function allows the form of the evolution of ΔH^+ with respect to the phase difference to be adjusted by the intermediary of the exponent n_θ (Fig. 7, curves 3).

This formulation (Eqs. (17) and (18)) introduces only three supplementary parameters, b_θ, Y_θ^{sat} and n_θ. However, since the deficit hardening is a function of the parameter δ, the coefficients Y_θ^{sat} and n_θ are not independent of the choice of this parameter.

Model 2: With the aid of simple geometric considerations, it can be shown that ΔH^- is approximately given by:

Table 2 Values of the model parameters (units s^{-1} and Nm^{-2})

$E = 1.45\ 10^{11}$ $\nu = 0.3$		Elasticity (Eq. (4))
$\dot{\epsilon}_0/(\sigma_0^*)^n = 2.7\ 10^{-23}$ $n = 2.2$ $C = 0.17$ $C^+ = 0.08$		State equation (Eqs. (5), (6))
$p_m = 10^4$ $p_1 = 1.8\ 10^3$ $p_2 = 3.5\ 10^2$ $\delta = 0.02$ $R_m = 8\ 10^2$ $\beta = 4\ 10^{-9}$ $M_1 = 2$ $M_0 = 4$ $\alpha_{ij}(0) = 0$		Kinematical variables (Eqs. (7), (15))
$b = 7$ $b^+ = 10$ $R = 7\ 10^{-34}$ $R^+ = 10^{-22}$ $R_0 = 4.7\ 10^{-9}$ $L_0 = 3.5$ $Y(0) = 3.64\ 10^7$		Scalar variables Y, Y^+ (Eqs. (8) and (9))
$\eta_{\text{sat}} = 3\ 10^{-2}$ $b_{\text{sat}} = 120$ $Y_\infty^{\text{sat}} = 11\ 10^7$ $Y^{\text{sat}+} = 18.6\ 10^7$ $Y^{\text{sat}}(0) = 7\ 10^7$		Memorization functions (Eqs. (11), (12))
$p^{(1)} = 100$ $\tau_{SN}^{(1)} = 6$ $Y^{(1)} = 0.116\ 10^7$ $\gamma_c = 1\ 10^{-7}$		Scalar interaction variable (Eqs. (13), (14))
Model (1) $b_\theta = b = 7$ $Y_\theta^{\text{sat}} = 4.70\ 10^7$ $n_\theta = 0.7$	Model (2) $b_\theta = b = 7$ $Y_\theta^{\text{sat}} = 2.4\ 10^7$ $n_\theta = 1$	Scalar nonradiality variable (Eqs. (17) to (20))

$$\Delta H^- = Y(3 - |\cos\beta| - \sqrt{3 + \cos^2\beta}), \text{ with } \cos\beta = \frac{\alpha_{ij}}{\bar{\alpha}}\frac{\alpha_{ij}^{(2)}}{\bar{\alpha}^{(2)}},$$

and this for the maximum value of the variable $\bar{\alpha}$ during the cycle. By distributing the weight of the hardening deficit in an identical fashion on the three kinematical components and by introducing it into the variable Y which describes the asymptotic state of each kinematical variable, a new definition of Y can be expressed as:

$$\left.\begin{aligned} &\dot{Y} = b(Y^{\text{sat}} g^*(\beta) - Y)[\dot{\bar{\epsilon}}^v - \ldots] \text{ with} \\ &g^*(\beta) = \left\{2 - \frac{1}{3}\left(|\cos\beta| + \sqrt{3 + \cos^2\beta}\right)\right\}_{\alpha^*} \end{aligned}\right\} \qquad (19)$$

$\bar{\alpha}^*$ is the maximum of the equivalent $\bar{\alpha}$ during a cycle. In this way it can be shown that independently of the phase difference and the parameter δ, nearly the same cyclic consolidation curve can be obtained. The supplementary hardening ΔH^* is then described by the function $f(\theta)$ such that:

$$f(\theta) = 1 - |\cos\theta|, \text{ (Idem Eq. (18) with } n_\theta = 1) \qquad (20)$$

This formulation (Eq. (17), (19), (20)) introduce only two supplementary parameters b_θ and Y_θ^{sat}. The totality of the model is constituted of the Eqs. (3) to (18) (model 1) or (3) to (17) and (19–20) (model 2) and its possibility are presented in Figs. 4 to 9. The calculations have been made with $b_\theta = b$ and cos $\theta = (\alpha_{ij}/\bar{\alpha}_{ij})/(\dot{\alpha}_{ij}/\dot{\bar{\alpha}})$, and the values of all the parameters are reported in Table 2. Figure 9 gives the simulation results of performed tests, which allows to draw the cyclic hardening curves (calculus with the model 1) and to deduce the evolution of ΔH^+ with respect to φ and R (Fig. 7, curves 3 for the model 1, and curves 4 for the model 2). Globally, the agreement is

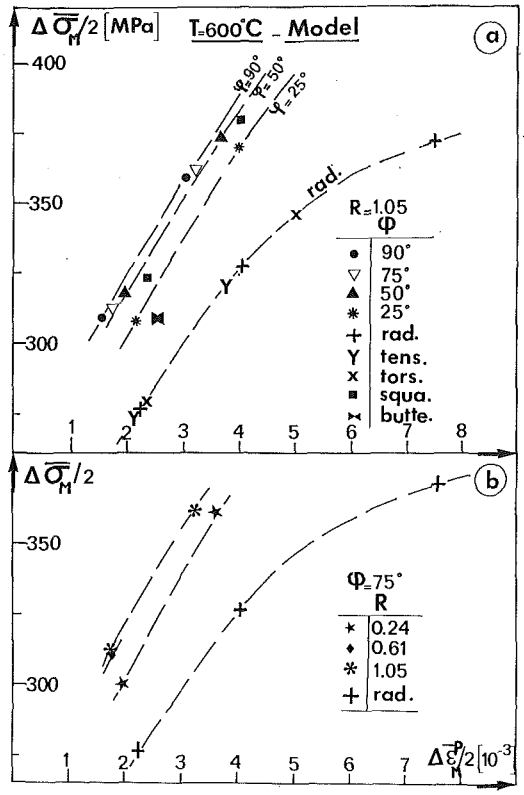

Fig. 9(*a*) Modelization of the influence of the phase difference on the cyclic hardening ($\Delta\bar{\sigma}_M/2 = f(\Delta\bar{\epsilon}^P_M/2)$). (*b*) Modelization of the effect of the parameter R on the cyclic hardening curve ($\Delta\bar{\sigma}_M/2 = f(\Delta\bar{\epsilon}^P_M/2)$).

satisfactory, especially considering that the experimentals errors reported in Fig. 7, due to the weakness of the supplementary hardening are not negligeable. ΔH^+ is a slightly increasing function of the amplitude $\Delta\epsilon^P_M/2$, which has not been observed experimentally. However, for lower temperatures, this dependence is clearly evident [15], [17] and its absence in the present study is due to the incremental technique that has been employed which can make a light softening appear under the second strain level. The results of the simulations for the three presented tests, are plotted in Figs. 4, 5, and 6. It is seen that globally the agreement is good. It is possible to take into account the significant decrease of ΔH^+ with the temperature by taking Y^{sat}_0 as a decreasing function of the temperature [48].

The simulations of 2-D ratchet with the non-radiality effect are reported in Fig. 8 (curves 3) and are nearly identical to those conducted earlier (curves 2), giving a global agreement.

The simulations show the capability of the present model to describe the observed effects. It can be noted that the formulation is part of a more general context of internal variable models [49] which have been widely developed since nearly fifteen years [12], [23], [28], [32], [44], [46], [50]. Though these models are structurally similar, namely having a state equation and evolutionary equations containing kinematical and isotropic hardening variables with Bailey-Orowan type kinetics, this is not true of the number or the details of these equations [50].

The originaly in the present formulation, in the context of viscoplasticity with time effects, resides in the wide diversity of phenomena which can be described [23], [48], namely the effects related to the viscosity (monotonic tests at different rates, creep, relaxation), to time (recovery or hardening with time, depending on the isotherm under consideration) and to the cyclic loadings (uniaxial with or without a holding time at the maximum of cycles, prestrain memory effects, supplementary hardening due to out of phase multiaxial loadings).

The final objective of a detailed description of this material for different isotherms is to describe its behavior under cyclic anisothermal loadings, with one or two mechanical components, over a wide range of temperatures (20–650°C), and where all the terms can be activated successively [51–53]. Moreover, this material presents some memory effects which depend on its temperature history.

The two modules presented in this article have been developed with these remarks in mind and integrated into a relatively complex behavior law developed in previous works [23], [24], [48].

V Conclusions

The influences to the loading rates on the unidirectional cyclic behavior and of the nonradiality of the loadings on the bidirectional cyclic behavior, have been presented for an austenitic stainless steel at 600°C. In addition, several results are reported of tension-torsion ratchet tests, a weakly non-radial tests where one of the stress components is fixed.

A new phenomenological formulation is proposed taking into account the effects of loading rate, nonproportionality, and progressive strain. This formulation can be integrated in modular form into a unified viscoplastic model developed elsewhere. The simulations obtained after integration of the identified model conform globally to the experimental observations.

References

1 Lamba, H. S., and Sidebottom, O. M., ASME JOURNAL OF ENGINEERING MATERIAL TECHNOLOGY, Vol. 100, 1978, pp. 96–103.

2 Brown, M. W., and Miller, K. J., *Fat. Eng. Mat. and Structure*, Vol. 1, 1979, pp. 93–106.

3 Kanazawa, K., Miller, K. J., and Brown, M. W., *Fat. Eng. Mat. and Struct.*, Vol. 2, 1979, pp. 217–228.

4 Krempl, E., and Lu, H., ASME JOURNAL OF ENGINEERING MATERIAL TECHNOLOGY, Vol. 106, 1984, pp. 376–382.

5 Cailletaud, G., Kaczmarek, H., and Policella, H., *Mech. Mat.*, Vol. 3, 1984, pp. 333–347.

6 Nouailhas, D., Chaboche, J. L., Savalle, S., and Cailletaud, G., *Int. J. Plasticity*, Vol. 1, 1985, pp. 317–330.

7 Ohashi, Y., Tanaka, E., and Ooka, M., ASME JOURNAL OF ENGINEERING MATERIAL TECHNOLOGY, Vol. 107, 1985, pp. 286–292.

8 McDowell, D. L., ASME *Journal of Applied Mechanics*, Vol. 52, 1985, pp. 298–308.

9 Yao, D., and Krempl, E., *Int. J. Plasticity*, Vol. 1, 1985, pp. 259–274.

10 Ohashi, Y., Kawai, M., and Kaito, T., ASME JOURNAL OF ENGINEERING MATERIAL TECHNOLOGY, Vol. 107, 1985, pp. 101–109.

11 McDowell, D. L., ASME *Journal of Applied Mechanics*, Vol. 54, 1987, pp. 323–334.

12 Benallal, A., and Marquis, D., ASME JOURNAL OF ENGINEERING MATERIAL TECHNOLOGY, Vol. 109, 1987, pp. 326–336.

13 Benallal, A., Le Gallo, P., and Marquis, D., *Nucl. Eng. Design*, Vol. 114, 1989.

14 Krempl, E., and Lu, H., *Biaxial and Multiaxial Fatigue*, Eds. M. W. Brown and K. J. Miller, EGF Publication 3, MEP London, 1989, pp. 89–106.

15 Benallal, A., Cailletaud, G., Chaboche, J. L., Marquis, D., Nouilhas, D., and Rousset, M., *Biaxial and Multiaxial Fatigue*, Eds. M. W. Brown and K. J. Miller, EGF Publication 3, MEP London, 1989, pp. 107–129.

16 Murakami, S., Kawai, M., and Ohmi, Y., ASME JOURNAL OF ENGINEERING MATERIAL TECHNOLOGY, Vol. 111, 1989, pp. 278–285.

17 Murakami, S., Kawai, M., Aoki, K., and Ohmi, Y., ASME JOURNAL OF ENGINEERING MATERIAL TECHNOLOGY, Vol. 111, 1989, pp. 32–39.

18 Delobelle, P., *J. of Nucl. Mat.*, Vol. 166, 1989, pp. 364–378.

19 Cailletaud, G., Doquet, V., and Pineau, A., III. Int. Conf. on Biaxial/Multiaxial Fatigue, 3–6 April, 1989, Stuttgart, Vol. 1, pp. 25–39.

20 Atcholi, E. K., Thesis 38, Besançon, France, 1987.

21 Contesti, E., "Compte rendu GIS Rupture a Chaud," Etude 2B, 28/06, 1985.

22 Matteazzi, S., Piatti, G., and Boerman, D., "Mech. Behavior and Nuclear Applications of Stainless Steel at Elevated Temperature," Varèse 20–22 May 1981, Italy, Published by the Metals Society, London, 1982, pp. 194–202.

23 Delobelle, P., "Constitutive Laws of Plastic Deformation and Fracture," Ottawa, 29–31 May, 1989, Canada, pp. 31-1–31-9.

24 Delobelle, P., Rev. Phys. Appl. 25, 1990, pp. 977–999.

25 de Los Rios, E. R., Andrews, R. M., Brown, M. W., and Miller, K. J., "Biaxial and Multiaxial Fatigue," eds., M. W. Brown and K. J. Miller, EGF Publication 3, MEP London, 1989, pp. 659–682.

26 Remy, L., Pineau, A., and Thomas, B., *Mat. Sci. Eng.*, 36, 1978, pp. 47–63.

27 Chaboche, J. L., and Rousselier, G., ASME *Journal Press Vessel Technical*, Vol. 105, 1983, pp. 153–166.
28 Chaboche, J. L., *Int. J. of Plasticity*, Vol. 2, No. 2, 1986, pp. 149–188.
29 McDowell, D. L., and Moosbrugger, J. C., ASME PVP—Vol. 129, 1987, pp. 1–11.
30 Nouilhas, D., Cailletaud, G., Policella, H., Marquis, D., Dufailly, J., Bollinger, E., Lieurade, H. P., and Ribes, A., *Eng. Fract. Mech.*, Vol. 21, No. 4, 1985, pp. 887–895.
31 Chaboche, J. L., Dang Van K., and Cordier, G., SMIRT V, Div. L1/13, Berlin, Germany, 1979.
32 Ohno, N., ASME *Journal of Applied Mechanics*, Vol. 49, 1982, pp. 721–727.
33 Blanc, D., Thése ENSMP, Paris, France, 1986.
34 Rose, K. S., and Glover, S. G., Acta Metall., Vol. 14, 1966, pp. 1505–1516.
35 Barnby, J. T., J. of the Iron and Steel Inst., 1965, pp. 392–397.
36 Park, S. C., Beckerman, L. P., and Reed-Hill, R. E., *Metall. Trans. A.*, Vol. 14, 1983, pp. 463–469.
37 Billa, R., Thése. Besançon, France, 1989.
38 Miller, A. K., and Sherby, O. D., *Acta Metall.*, Vol. 26, 1978, pp. 289–304.
39 Schmidt, C. G., and Miller, A. K., *Res. Mech.*, Vol. 3, 1981, pp. 109–129.
40 Kocks, U. F., Cook, R. E., and Mulford, R. A., *Acta Metall.*, Vol. 33, No. 4, 1985, pp. 623–638.
41 Burlet, H., and Cailletaud, G., *Eng. Comput.*, Vol. 3, 1986, pp. 143–153.
42 Delobelle, P., unpublished works, 1989.
43 Rousset, M., Thése Paris, 1985.
44 Bodner, S. R., "Unified Constitutive Equations for Creep, Plasticity," Ed. by, A. K. Miller, Elsevier Applied Science, 1987, pp. 273–301.
45 Benallal, A., Le Gallo, P., and Marquis, D., *Proceedings of Mecamat International Seminar on the Inelastic Behaviour of Solids, Models and Utilization*, August 30–September 1, Besancon, France, 1988, V/361–371.
46 McDowell, D. L., and Moosbrugger, J. C., Proceedings of Mecamat "International Seminar on the Inelastic Behaviour of Solids: Models, and Utilization," 30 August–September 1, Besançon, France, 1988, pp. 547–574.
47 Chaboche, J. L., and Nouailhas, D., ASME JOURNAL OF ENGINEERING MATERIALS AND TECHNOLOGY, Vol. 111, 1989, pp. 384–392.
48 Delobelle, P., "Synthesis of the Elastoviscoplastic Behavior and Modelization of an Austenitic Stainless Steel over a Large Temperature Range, Under Uniaxial and Biaxial Loadings, Part I: Behavior, Part II: Phenomenological Modelization," to appear in *Int. J. of Plasticity*, 1993.
49 Halphen, B., and Quoc-Son, N., *J. Mec. Theor.*, Vol. 14, No. 1, 1975, p. 39.
50 Walker, K. P., NASA Report, n° CR 165 533, 1981.
51 Ohno, N., Takahashi, Y., and Kuwabara, K., ASME JOURNAL OF ENGINEERING MATERIALS AND TECHNOLOGY, Vol. 111, 1989, p. 106.
52 Chan, K. S., and Lindholm, U. S., ASME JOURNAL OF ENGINEERING MATERIALS AND TECHNOLOGY, Vol. 112, 1990, p. 15.
53 Bouchou, A., and Delobelle, P., to be published in 1993.